AIP | Journal of Applied Physics

Ion irradiation synthesis of Ag–Au bimetallic nanospheroids in SiO2 glass substrate with tunable surface plasmon resonance frequency

Xuan Meng, Tamaki Shibayama, Ruixuan Yu, Shinya Takayanagi, and Seiichi Watanabe

Citation: J. Appl. Phys. **114**, 054308 (2013); doi: 10.1063/1.4817725
View online: http://dx.doi.org/10.1063/1.4817725
View Table of Contents: http://jap.aip.org/resource/1/JAPIAU/v114/i5
Published by the AIP Publishing LLC.

JOURNAL OF APPLIED PHYSICS **114**, 054308 (2013)

Ion irradiation synthesis of Ag–Au bimetallic nanospheroids in SiO_2 glass substrate with tunable surface plasmon resonance frequency

Xuan Meng,[1] Tamaki Shibayama,[2,a)] Ruixuan Yu,[1] Shinya Takayanagi,[1] and Seiichi Watanabe[2]
[1]*Graduate School of Engineering, Hokkaido University, Sapporo, Hokkaido 060–8628, Japan*
[2]*Center for Advanced Research of Energy and Materials, Faculty of Engineering, Hokkaido University, Sapporo, Hokkaido 060–8628, Japan*

(Received 25 March 2013; accepted 23 July 2013; published online 5 August 2013)

Ag–Au bimetallic nanospheroids with tunable localized surface plasmon resonance (LSPR) were synthesized by 100 keV Ar–ion irradiation of 30 nm Ag–Au bimetallic films deposited on SiO_2 glass substrates. A shift of the LSPR peaks toward shorter wavelengths was observed up to an irradiation fluence of 1.0×10^{17} cm^{-2}, and then shifted toward the longer wavelength because of the increase of fragment volume under ion irradiation. Further control of LSPR frequency over a wider range was realized by modifying the chemical components. The resulting LSPR frequencies lie between that of the pure components, and an approximate linear shift of the LSPR toward the longer wavelength with the Au concentration was achieved, which is in good agreement with the theoretical calculations based on Gans theory. In addition, the surface morphology and compositions were examined with a scanning electron microscope equipped with an energy dispersive spectrometer, and microstructural characterizations were performed using a transmission electron microscope. The formation of isolated photosensitive Ag–Au nanospheroids with a FCC structure partially embedded in the SiO_2 substrate was confirmed, which has a potential application in solid-state devices. © *2013 AIP Publishing LLC*. [http://dx.doi.org/10.1063/1.4817725]

I. INTRODUCTION

Physical and chemical properties of low-dimensional solid-state systems have attracted considerable attention because of their technological significance.[1–12] The best-known optical property of metal nanoparticles embedded in glass is the intense absorption band in the visible spectrum arising from a collective excitation of the free electrons. This is called the localized surface-plasmon resonance (LSPR), and the formal explanation of this remarkable phenomenon was given by Gustav Mie.[9,13] Metallic nanoparticles have been extensively studied both experimentally and theoretically[1–16] because of their appreciable applications in LSPR-based biological and chemical sensors such as molecular, gas, and pH sensors.

There is currently increasing interest in developing low-cost, reproducible, and efficient plasmonic sensors based on spectral peak shift.[3–12] It has been demonstrated that particle size, shape, and component material play important roles in determining the sensitivity.[17–19] There has been a great deal of research conducted on controlling the morphology and composition of these nanoparticles.[17–27] The synergistic control of various parameters sensitive to the LSPR band includes both particle size and shape.[17–23] Further control of LSPR frequency over a wider range has been achieved by synthesizing bimetallic nanoparticles fabricated in the form of alloys of two metals. In general, the resulting LSPR frequency lies in between that of the pure components, and depends on the relative amounts of the two components.[23–27] In particular, Ag–Au nanocomposites have attracted increasing interest because of their composition-dependent tunable optical properties and because complete miscibility of Au and Ag can be obtained at any composition in both bulk materials and NPs.[18,19,21,24–27] To date, Ag–Au bimetallic NPs showing a single LSPR band tuned over the entire wavelength region in between that of pure Ag and Au have been synthesized.

There have been impressive developments in the field of nanotechnology in recent years, with chemical and lithographical methodologies being developed to synthesize NPs of particular size and shape. Purely chemical synthetic routes such as innovative colloidal self-assembly,[18–20,24,26] lithography methods such as electron beam lithography[28] and nanosphere lithography,[27,29] thermal deposition,[25] laser irradiation,[30] ion implantation and consequent annealing,[31,32] and ion irradiation and subsequent annealing[33–35] have been developed for manufacturing high efficiency platforms for the LSPR-based sensors. Nowadays, colloidal chemistry can produce a myriad of metal NPs in solutions with a variety of morphologies from sphere to complex core-shell, with very good control of the size distribution;[17–23] this control over the size, composition, and morphology of the NPs in a system can produce dramatically different absorption features in the visible or near-infrared spectrum. However, the synthesis of these structures, in particular within a matrix, is a significant challenge. This is especially true if they are to be used in solid-state devices such as biosensors, in which advanced surface functionalization of the NPs is in active state is required.

To overcome these problems, low-energy ion modification in metal–silica systems can be employed. Low-energy ions (up to few hundred keV) undergo unclear stopping and

a)Author to whom correspondence should be addressed. Electronic mail: shiba@qe.eng.hokudai.ac.jp

the energy deposition is dominated by nuclear energy loss, which can effectively induce mass transfer and results in irradiation enhanced diffusion. This in turn leads to lateral transport of metal atoms and therefore the dewetting of thin metal films.[34,36] Furthermore, this effectively burrows the nanostructures into the dielectric matrix because of the ion-induced viscous flow, and subsequently improves the adhesion of the deposited metal films on insulating substrates.[37,38] Previously, we have synthesized photosensitive gold NPs partially embedded in SiO_2 glass substrates.[35] In this paper, we report a synthesis method of Ag–Au alloy nanospheroids in SiO_2 glass substrate by ion irradiation and its tunable optical properties. In this method, the synthesized nanoparticles with advanced functionalization surface partially embedded in the dielectric matrix were obtained.

II. EXPERIMENTAL PROCEDURE

Ar–ion irradiation induced surface nanostructuring of Ag–Au bimetallics with various molar ratios deposited on SiO_2 substrate was performed, and tunable plasmon resonance frequency was obtained. Ag–Au bimetallic thin films were thermally evaporated on mirror polished SiO_2 substrates at ambient temperature by electrically heating the Ag and Au sources under a 6.0×10^{-5} Torr vacuum. In general, the Ag nanostructures are unstable and easily get oxidized.[39–41] Therefore, the as-deposited samples were kept in the vacuum condition. However, a strong increase in the oxidation resistance was observed with the increase of Au atomic fraction inside the nanostructures,[41] and it is reported that most of the Au–Ag nanostructures was not oxidized at gold fractions above 0.4 in solution.[42] Therefore, the Au–Ag bimetallic films on SiO_2 substrates were thought to be stable in this study. The film thickness was verified by transmission electron microscope (TEM; JEOL JEM–2010F), and a field–emission scanning electron microscope (SEM; JEOL JSM–7001FA) equipped with energy dispersive spectrometer (EDS; Noran Thermo Fischer Scientific) was used for measuring the compositions of the as-deposited and irradiated samples.

For the 30 nm $Ag_{(50\%)}$–$Au_{(50\%)}$ bimetallic films deposited on the SiO_2 substrates, the optical micrograph exhibits a blue color (Fig. 1(a), upper section) and the surface is uniformly smooth and consists of planar grains as small as a few nanometers in size (SEM micrograph in Fig. 1(a), lower section). 100 keV Ar ions irradiation at ambient temperature with fluences of $4.0 \times 10^{16}\,cm^{-2}$, $5.5 \times 10^{16}\,cm^{-2}$, $7.0 \times 10^{16}\,cm^{-2}$, $1.0 \times 10^{17}\,cm^{-2}$, and $1.4 \times 10^{17}\,cm^{-2}$ was performed to study the fluence dependence. The energies of the ions were chosen such that the range is wider than the thickness of the bimetallic layer, as calculated by the SRIM 2011 code.[43] Ar–ion irradiation on the samples was performed using the 400 keV ion accelerator at the High Voltage Electron Microscope Laboratory, Hokkaido University.[44] A low pressure of 10^{-3} Pa was maintained inside the irradiation chamber. To ensure uniform irradiation, Ar–ion beam was scanned and the current was maintained at approximately 2.0 $\mu A\,cm^{-2}$. Furthermore, on top of the SiO_2 samples, pure silver, pure gold, and three different bimetallic Ag–Au films with molar ratios of 0.25:0.75, 0.5:0.5, and 0.75:0.25 were deposited to investigate the component dependence, and consequent Ar–ion irradiation of these bimetallic films was also performed to a fluence of $1.0 \times 10^{17}\,cm^{-2}$. For the as-deposited samples, the color changed from blue to yellow green (upper sections of Figs. 5(a)–5(e)) and the surface remained uniformly smooth (lower section of Figs. 5(a)–5(e)).

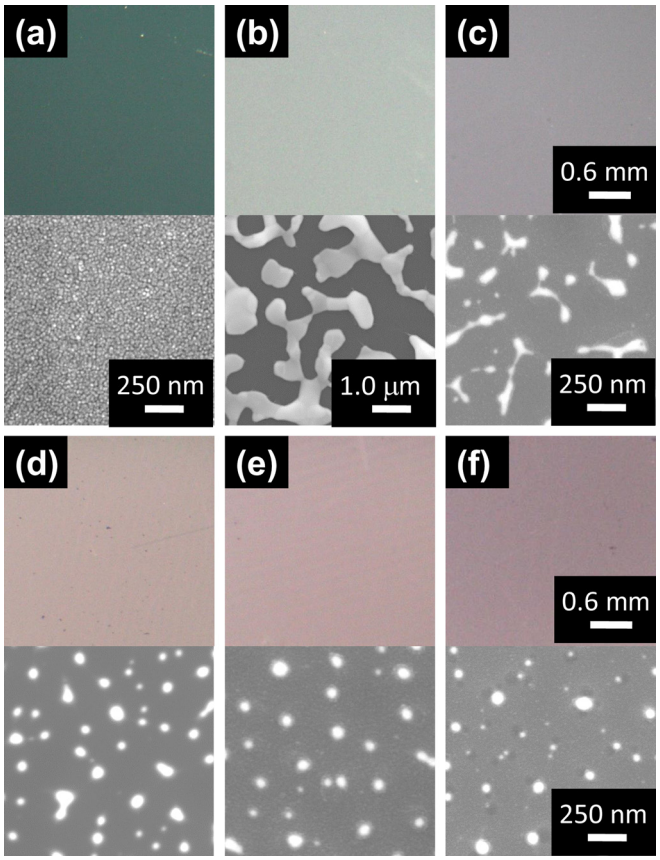

FIG. 1. Optical micrographs (upper sections of each panel) and SEM micrographs (lower sections of each panel) of (a) $Ag_{50\%}$–$Au_{50\%}$ as-deposited SiO_2, (b) thermally annealed sample, and post-irradiation annealed samples with irradiation fluences of (c) $4.0 \times 10^{16}\,cm^{-2}$, (d) $7.0 \times 10^{16}\,cm^{-2}$, (e) $1.0 \times 10^{17}\,cm^{-2}$, and (f) $1.4 \times 10^{17}\,cm^{-2}$.

As the radiation induced defects can be removed by annealing at temperatures higher than 623 K,[45] post-irradiation thermal annealing is usually employed to anneal ion irradiated samples. Therefore, thermal annealing was conducted *ex situ* under high vacuum (4.25×10^{-5} Pa) at 773 K for 2 h. After that, optical absorption spectra were recorded over a wavelength range of 300–800 nm on a spectrophotometer (JASCO V–630) with a spectral bandwidth of 1 nm, and the SEM observations were used to examine the surface modification. The line and surface element concentration were evaluated at the nanoscale using the SEM coupled with an EDS, and the line chemical concentration profiles across the surface were obtained using the SEM operated at 6.0 keV. Moreover, microstructural characterization was performed using the TEM operated at 200 keV. The cross-sectional TEM samples were prepared using a precision ion polishing system (PIPS; JEOL AT–12310), and ion milling was performed using a cold stage to avoid undesired thermal modification of the samples.

III. RESULTS

A. Fluence effect on surface nanostructuring by ion irradiation

The morphology of the surface nanostructuring by ion irradiation on the dielectric substrate depends on variations in the irradiation parameters such as fluence, current, and beam energy. In this study, fluence dependence on the ion induced surface nanostructure was studied using 100 keV Ar–ion irradiation of 30 nm $Ag_{(50\%)}$–$Au_{(50\%)}$ bimetallic films deposited on SiO_2 substrates with the irradiation fluence increasing from $4.0 \times 10^{16}\,cm^{-2}$ to $1.4 \times 10^{17}\,cm^{-2}$. A color change from dark green to light violet was observed, as can be observed in the optical micrographs in the upper sections of Fig. 1. SEM was used to study the surface nanostructure after the post-irradiation thermal annealing. The lower sections of each panel in Figure 1 show SEM micrographs of (a) as-deposited $Ag_{(50\%)}$–$Au_{(50\%)}/SiO_2$, (b) annealed sample, and post-irradiation annealed samples with irradiation fluences of (c) $4.0 \times 10^{16}\,cm^{-2}$, (d) $7.0 \times 10^{16}\,cm^{-2}$, (e) $1.0 \times 10^{17}\,cm^{-2}$, and (f) $1.4 \times 10^{17}\,cm^{-2}$. For the specimen irradiated at the lowest fluence ($4.0 \times 10^{16}\,cm^{-2}$), the line profiles of the chemical concentration across the surface were obtained (Fig. 2). Figure 2(a) shows the typical SEM image, and the red line indicates the line along which the element concentration was determined. Fig. 2(b) shows the line profile of silica and oxygen concentrations. Fig. 2(c) shows the line profile of silver and gold concentrations with the Ag peaks appearing in the same place as the Au peaks; both peaks occur at valleys in the silica and oxygen profiles, and the peaks in the concentration profiles correspond to the bright areas shown in Fig. 2(a), indicating that silver and gold alloyed at the nanoscale. Therefore, the bright contrast areas in the SEM micrographs represent the retained bimetallic films on the substrates.

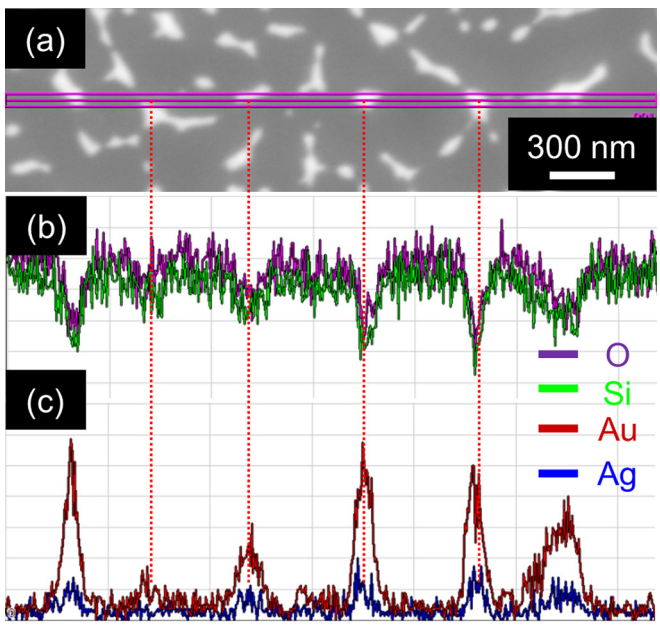

FIG. 2. (a) Typical SEM micrograph of post-irradiation annealed sample of $Ag_{50\%}$–$Au_{50\%}$ bimetallic film on SiO_2 at a fluence of $4.0 \times 10^{16}/cm^2$; (b) line profiles of silica and oxygen along the horizontal line indicated in (a); and (c) line profiles of silver and gold along the horizontal line indicated in (a).

While the surface of the as-deposited SiO_2 substrate is smooth with fine particles a few nanometers in size (lower section of Fig. 1(a)), relatively large polygonal pitches with a Heywood diameter greater than 900 nm were observed (lower section of Fig. 1(b)) after thermal annealing because of the thermal induced homogeneous nucleation.[28,46] As-deposited SiO_2 is quite different from the ion irradiated samples. With increasing irradiation fluence, the process of bimetallic film evolution under Ar–ion irradiation is clearly observed, with the formation of isolated photosensitive nanospheroids. Partially connected nanoscale islands formed after irradiation to a fluence of $4.0 \times 10^{16}\,cm^{-2}$ because of ion induced dewetting of thin metallic films.[34] When the dose increased to $7.0 \times 10^{16}\,cm^{-2}$, elongated nanospheroids were obtained on the substrate. A detailed study of the $Ag_{(50\%)}$–$Au_{(50\%)}$ bimetallic nanospheroids was conducted by measuring the nanospheroids diameter and aspect ratio, and the results are summarized in Table I. Figure 3(a) illustrates the mean diameter and aspect ratio of the $Ag_{(50\%)}$–$Au_{(50\%)}$ nanospheroids as a function of irradiation fluence. Both show a systematic decrease with the irradiation fluence, and their deviations also decrease with the irradiation fluence. Bright field cross-sectional TEM micrograph of these nanospheroids was obtained (Fig. 4(a)), and the diffraction pattern for a typical nanospheroid is given in Fig. 4(b) showing a FCC structure. As observed in this figure, the nanospheroids are partially embedded in the substrate, and the mechanism of the embedment has been studied in detail by Klimmer *et al.*[38] It has been concluded that these nanospheroids are embedded by irradiation induced viscous flow, considering the effect of surface sputtering.[38]

Optical absorption spectra were recorded for each specimen after irradiation. Figure 3(b) shows the absorption spectra of the samples irradiated at fluences ranging from $4.0 \times 10^{16}\,cm^{-2}$ to $1.4 \times 10^{17}\,cm^{-2}$. For the specimen irradiated at a fluence of $4.0 \times 10^{16}\,cm^{-2}$, a broad absorption peak was observed, while narrower absorption peaks were clearly observed for specimens irradiated at fluences exceeding $7.0 \times 10^{16}\,cm^{-2}$. These absorption peaks were induced by the resonance of the incident light with the combined oscillation of the free electrons aggregated at the surface of these

TABLE I. Statistical analysis of morphology and optical properties for post-irradiation thermal annealed $Ag_{(50\%)}$–$Au_{(50\%)}/SiO_2$ at various fluences.

Fluence ($\times 10^{16}\,cm^{-2}$)	d[a] (nm)	Aspect ratio[b]	LSPR[c] (nm)	LSPR[d] (nm)
4.0	64.3 ± 27.4	1.94 ± 0.79	565.0 ± 3.0	587
5.5	56.5 ± 25.5	1.67 ± 0.69	526.0 ± 0.5	552
7.0	50.4 ± 19.5	1.37 ± 0.47	500.0 ± 0.4	511
10.0	50.3 ± 19.5	1.24 ± 0.28	498.2 ± 0.4	494
14.0	46.1 ± 18.8	1.15 ± 0.17	522.0 ± 0.3	483

[a]d is the mean diameter of $Ag_{(50\%)}$–$Au_{(50\%)}$ bimetallic nanospheroids.
[b]Aspect ratio is the mean aspect ratio of $Ag_{(50\%)}$–$Au_{(50\%)}$ bimetallic nanospheroids.
[c]LSPR is the measured maximum absorption of the LSPR band of $Ag_{(50\%)}$–$Au_{(50\%)}$ bimetallic nanospheroids.
[d]LSPR is the calculated maximum absorption of the LSPR band of $Ag_{(50\%)}$–$Au_{(50\%)}$ bimetallic nanospheroids.

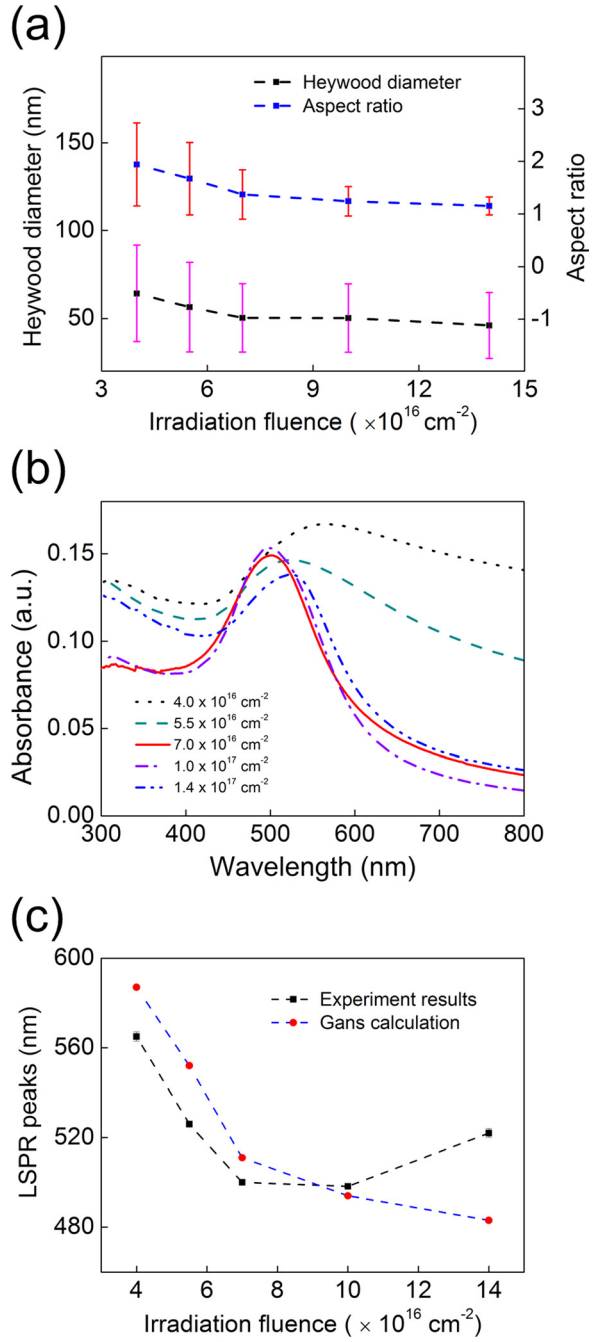

FIG. 3. (a) Heywood diameters and aspect ratios of the nanospheroids plotted against the irradiation fluence; (b) photoabsorbance spectra of the samples after post-irradiation thermal annealing; and (c) experimentally measured and Gans calculation of the maximum absorption wavelength position plotted against irradiation fluence.

$Ag_{(50\%)}$–$Au_{(50\%)}$ bimetallic nanospheroids partially embedded in the SiO_2 substrate. This enhanced absorption is a characteristic of LSPR, and the peak positions are summarized in Table I. These absorbance bands correspond to the LSPR peak exhibited by Ag–Au bimetallic nanospheroids sustained on or embedded in a SiO_2 matrix.[22,24–27] As the irradiation fluence of the Ar ions increased, a shift of the LSPR peak positions toward the short wavelength was observed up to an irradiation fluence of $1.0 \times 10^{17}\,cm^{-2}$, and then shifted towards the longer wavelength with further increase of the fluence (Fig. 3(c)).

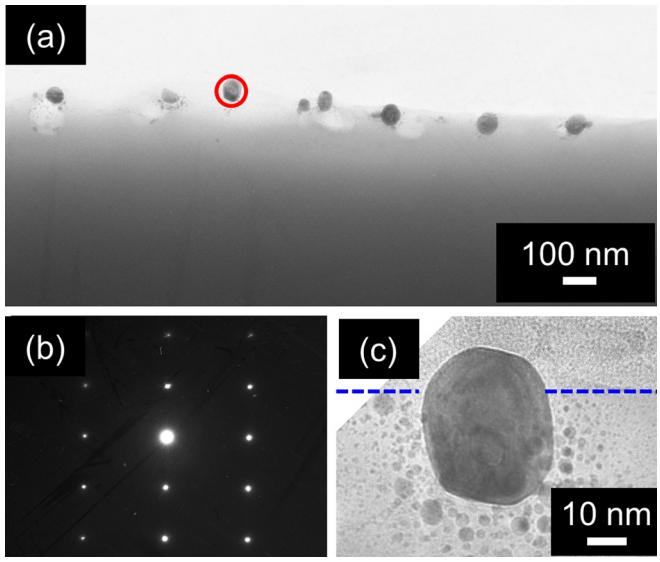

FIG. 4. (a) Typical bright field cross-sectional TEM micrograph of $Ag_{(50\%)}$–$Au_{(50\%)}$ bimetallic nanospheroids partially embedded in SiO_2 substrate fabricated by post-irradiation annealing of $Ag_{(50\%)}$–$Au_{(50\%)}$/SiO_2 irradiated to a fluence of $1.0 \times 10^{17}\,cm^{-2}$. (b) Diffraction pattern for a typical $Ag_{(50\%)}$–$Au_{(50\%)}$ bimetallic nanospheroid circled in (a). (c) High magnification TEM micrograph for a typical $Ag_{(50\%)}$–$Au_{(50\%)}$ bimetallic nanospheroid circled in (a) with the dashed blue line indicating the interface between SiO_2 substrate and vacancy.

B. Ag–Au nanospheroids with tunable surface plasmon resonance frequency

Bimetallic nanospheroids with various Au–Ag molar ratios (0.0:1.0, 0.25:0.75, 0.5:0.5, 0.75:0.25, 1.0:0.0) were synthesized using Ar–ion irradiation of Au–Ag bimetallic films deposited on SiO_2 substrates. A color change from light yellow to violet was observed by optical microscope for the five samples (upper sections of Figs. 5(a')–5(e')). SEM was used to study the surface nanostructuring after post-irradiation thermal annealing. SEM micrographs (lower sections of Figs. 5(a')–5(e')) show the surface morphology of the post-irradiation annealed samples of pure silver, $Ag_{(75\%)}$–$Au_{(25\%)}$, $Ag_{(50\%)}$–$Au_{(50\%)}$, $Ag_{(25\%)}$–$Au_{(75\%)}$, and pure gold deposited on SiO_2 substrates. A detailed study of the $Ag_{(X\%)}$–$Au_{(100\text{-}X\%)}$ bimetallic nanospheroids was conducted by measuring the nanospheroids diameter and aspect ratio, and the results are summarized in Table II. Figure 6(a) illustrates the mean diameter and aspect ratio of the Ag–Au nanospheroids as a function of Au concentration, which shows the formation of nanospheroids with comparable size and aspect ratio for the five samples.

Optical absorption spectra were recorded for each specimen after post-irradiation annealing. Figure 6(b) shows the tunable characteristics of LSPR frequency of Ag–Au bimetallic nanospheroids of all five samples, and a single localized surface plasmon absorption band for each sample was observed. Figure 6(c) shows the UV–vis absorption peak position plotted against the percentage of Au concentrations. This figure demonstrates that the LSPR peak positions shift approximately linearly from 424.5 nm (Ag nanospheroids) to 566.6 nm (Au nanospheroids) with an increase in Au molar fractions. The wavelength of the maximum absorption band for each sample is summarized in Table II. In this study, the

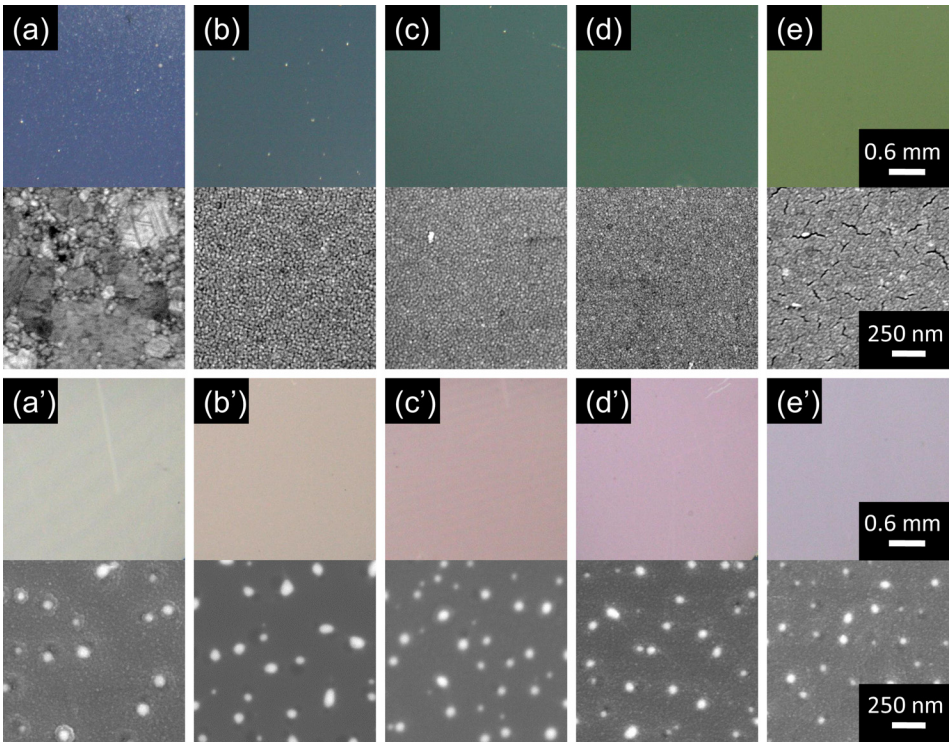

FIG. 5. Optical micrographs (upper section of each panel) and SEM micrographs (lower section of each panel) of (a) pure silver, (b) $Ag_{(75\%)}$–$Au_{(25\%)}$, (c) $Ag_{(50\%)}$–$Au_{(50\%)}$, (d) $Ag_{(25\%)}$–$Au_{(75\%)}$, and (e) pure gold as-deposited on SiO_2. Figures 5(a')–5(e') are optical micrographs and SEM micrograph of these five samples after post-irradiation thermal annealing.

nanospheroids were synthesized in the vacuum chamber. However, *ex situ* photoabsorption spectra measurement was carried out in air. Therefore, a layer of oxide Ag (usually Ag_2O) was formed on the nanospheroids surface, and the Ag–core Ag–oxide shell structure will induce a red shift of the characteristic surface plasmon resonance response for pure Ag, which located at around 400 nm.[39,40] However, this plasmon absorption peak was rather stable over time: after 8 months in a low vacuum condition, the plasmon absorption intensity has decreased a little (see S1 in the supplementary information[47]).

IV. DISCUSSIONS

In general, the optical property of nanoparticles is characterized by photoabsorbance A. The photoabsorbance A is proportional to the extinction cross-section σ_{ext}, which can be obtained by the Mie scattering theory.[9,13] However, Mie theory is only applicable to spherical particles. Richard Gans generalized Mie's results to spheroidal particles of any aspect ratio in the small particle approximation.[8,13] In the case of a single uncharged spheroidal particle with dielectric function $\varepsilon = \varepsilon_1 + i\varepsilon_2$ dispersed in a surrounding medium with dielectric function ε_m. The general expression of the extinction cross-section takes the following form:

$$\sigma_{ext} = \frac{2\pi\varepsilon_m^{3/2}V}{3\lambda}\sum_{j=1}^{3}\frac{(1/p_j^2)\varepsilon_2}{\{\varepsilon_1 + [(1-p_j)/p_j]\varepsilon_m\}^2 + \varepsilon_2^2}, \quad (1)$$

where λ the incident light wavelength, V the particle volume, and $\varepsilon = \varepsilon_1 + i\varepsilon_2$ the size-dependent complex dielectric function of the particle.

Equation (1) is valid if the particle size is much smaller compared to the light wavelength λ. Here, P_j includes P_A, P_B, and P_C, termed depolarization factors, for each axis of the particle. In our study, $A > B = C$ is assumed for a prolate spheroid. The depolarization factors anisotropically alter the values of ε_1 and ε_2, and therefore the resulting LSPR peak frequencies. The depolarization factors are given as follows:

$$P_A = \frac{1-e^2}{e^2}\left[\frac{1}{2e}\ln\left(\frac{1+e}{1-e}\right) - 1\right], \quad (2a)$$

$$P_B = P_C = (1 - P_A)/2, \quad (2b)$$

where e is the following factor, which includes the particle aspect ratio R:

$$e = [1 - (B/A)^2]^{1/2} = (1 - 1/R^2)^{1/2}. \quad (3)$$

The LSPR absorption holds when the denominator in Eq. (1) exhibits a minimum, that is

TABLE II. Statistical analysis of morphology and optical properties for post-irradiation thermal annealed $Ag_{(X\%)}$–$Au_{(100-X\%)}/SiO_2$ at a fluence of $1.0 \times 10^{17}\,cm^{-2}$.

Samples	d[a]	Aspect ratio[b]	LSPR[c] (nm)	LSPR[d] (nm)
Ag/SiO_2	48.3 ± 20.0	1.24 ± 0.33	424.5 ± 2.5	452
$Ag_{(75\%)}$–$Au_{(25\%)}/SiO_2$	51.7 ± 19.1	1.20 ± 0.20	486.3 ± 0.2	473
$Ag_{(50\%)}$–$Au_{(50\%)}/SiO_2$	50.3 ± 19.5	1.24 ± 0.28	498.2 ± 0.4	494
$Ag_{(25\%)}$–$Au_{(75\%)}/SiO_2$	45.2 ± 19.5	1.33 ± 0.43	538.5 ± 0.2	522
Au/SiO_2	37.5 ± 15.0	1.18 ± 0.19	566.6 ± 0.4	521

[a]d is the mean diameter of $Ag_{(X\%)}$–$Au_{(100-X\%)}$ bimetallic nanospheroids.
[b]Aspect ratio is the mean aspect ratio of $Ag_{(X\%)}$–$Au_{(100-X\%)}$ bimetallic nanospheroids.
[c]LSPR is the measured maximum absorption of the LSPR band of $Ag_{(X\%)}$–$Au_{(100-X\%)}$ bimetallic nanospheroids.
[d]LSPR is the calculated maximum absorption of the LSPR band of $Ag_{(X\%)}$–$Au_{(100-X\%)}$ bimetallic nanospheroids.

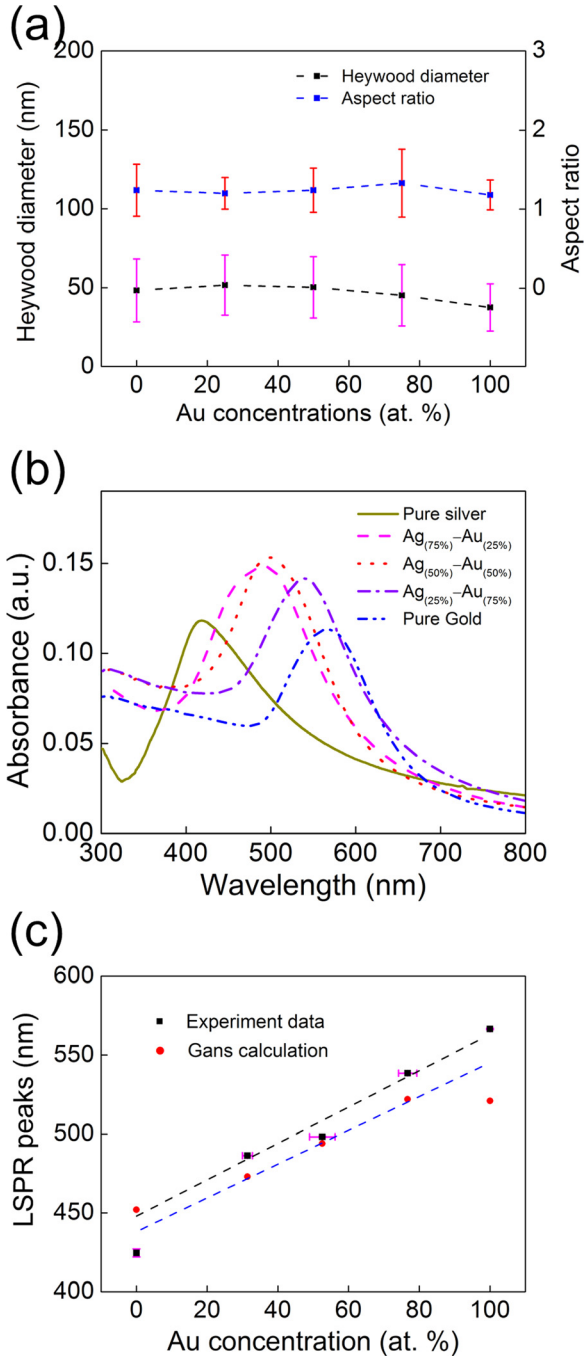

FIG. 6. (a) Heywood diameters and aspect ratios of the $Ag_{(X\%)}$–$Au_{(100\text{-}X\%)}$/SiO_2 nanospheroids plotted against the Au concentration; (b) photoabsorbance spectra of the samples after post-irradiation thermal annealing; and (c) experimentally measured and Gans calculation of the maximum absorption wavelength position plotted against the Au concentration, and the dashed lines are used for guiding the eyes only.

$$\varepsilon_1 = -[(1-P_j)/P_j]\varepsilon_m. \tag{4}$$

In particular, for noble-metal NPs the equation has a solution in the visible range at the LSPR frequency, because the real part of the dielectric function is negative. The extinction spectrum from Eq. (1) has two peaks, one corresponding to the transverse plasmon mode and the other corresponding to the longitudinal plasmon mode. Equation (1) provides an intuitive understanding of the effects of aspect ratio on the LSPR peak wavelength. The factor $(1-P_j)/P_j$ increases with aspect ratio and can be greater than 2, leading to a shift of the LSPR peak towards the longer wavelength. For nanoparticles other than these spheres and spheroids, particle shape plays a significant role on the LSPR spectra. However, this cannot be determined by analytical analysis, and must be studied numerically. Numerical methods for plasmonic nanoparticles include the Mie–Maxwell–Garnett (MMG) method, the generalized multisphere Mie (GMM) theory,[22] the discrete dipole approximation (DDA),[14] and the Finite-Difference Time-Domain (FDTD) method.[48]

An extension of Gans theory for the calculation of optical absorption spectra in bimetallic nanoparticles has been developed. While dealing with the optical properties of alloyed metal nanoclusters, the most important aspect is the correct choice of the alloyed nanoparticle dielectric function. The bimetallic nanoparticle dielectric function is assumed to be a weighted linear combination of dielectric functions for single particles. It can be calculated in terms of the dielectric functions ε_{Ag} and ε_{Au} for nanoparticles of the same size consisting of the pure metals[24,49]

$$\varepsilon_{Alloy} = \alpha\varepsilon_{Ag} + (1-\alpha)\varepsilon_{Au}, \tag{5}$$

where α the relative volume concentration of Ag inside the nanoparticle.

The important quantity in Eqs. (1) and (5) is the nanoparticles dielectric function ε, which differs from that of the bulk metals. It has been shown that the noble metals gold and silver cannot be treated as a free electron gas, in which the dielectric function can be written within the Drude formula. It is generally accepted that a good approximation of the dielectric function of small particles is obtained from the bulk dielectric function, considering the contributions of the interband contributions.[49,50] Consequently, the dielectric function is written as

$$\varepsilon = \varepsilon_1 + i\varepsilon_2, \tag{6}$$

$$\varepsilon_{1,2} = \varepsilon^D_{1,2} + \chi^{IB}_{1,2}, \tag{7a}$$

$$\varepsilon^D_1 = 1 - \omega_p^2/(\omega^2+\gamma^2), \tag{7b}$$

$$\varepsilon^D_2 = \omega_p^2\gamma/[\omega(\omega^2+\gamma^2)], \tag{7c}$$

where $\varepsilon^D_{1,2}$ and $\chi^{IB}_{1,2}$ are the real and imaginary parts of the free electrons and interband contributions into ε, ω_p is the plasma frequency, and γ the rate of electron collisions. Silver and gold have close bulk plasma frequencies: $\hbar\omega_P = 8.5\,\text{eV}$ for silver and $\hbar\omega_P = 9.0\,\text{eV}$ for gold, and $\hbar$ is the reduced Planck constant.[49,51] As the particle size reduces, the rate of scattering from the particle surface γ_s becomes larger than the bulk scattering γ_0, and the following relation can be obtained:[9,49–52]

$$\gamma = \gamma_0 + \frac{aV_F}{r}, \tag{8}$$

where V_F is the Fermi velocity and r is the particle radius. For gold and silver, the Fermi velocity gets almost the same

value $V_F = 1.4\,\text{nm fs}^{-1}$, $\hbar\gamma_0 = 0.021\,\text{eV}$ (Ref. 52), and 0.07 eV (Ref. 51) for silver and gold, respectively. The coefficient a in Eq. (8) usually takes the value of unity,[49] which is actually used to consider some of the other factors like electron density at the surface. Therefore, the differences between the dielectric functions of nanoparticles and bulk metals are included in the free electron part of the dielectric function. The contribution arising from interband transitions is assumed to be unchanged. The analytical calculation of interband dielectric function is complicated. However, it is possible to approximate the real interband part of the dielectric function χ_1^{IB} by using the appropriate values. In the present calculations, the interband dielectric functions were extracted from pure gold and silver nanoparticles with diameters of several tens of nanometers[50]

$$\chi_1^{IB}(Ag) = Re(\chi_{Ag}^{IB}) = 2.25 \pm 0.1, \tag{9a}$$

$$\chi_1^{IB}(Au) = Re(\chi_{Au}^{IB}) = 7.2 \pm 0.1. \tag{9b}$$

In general, if the imaginary interband part of the dielectric function χ_2^{IB} is much smaller than the real part χ_1^{IB}, the following expression for the resonance frequency can be obtained from Eq. (1):

$$\omega_R = \left(\frac{\omega_p^2}{1 + \chi_1^{IB} + [(1 - P_j)/P_j]\varepsilon_m} - \gamma^2 \right)^{1/2}, \tag{10}$$

where ω_R is the LSPR peak frequency. Converting from frequency to wavelength via $\lambda = 2\pi c/\omega_R$, the LSPR peak wavelengths can be obtained as follows:

$$\lambda_R = 2\pi c \left(\frac{\omega_p^2}{1 + \chi_1^{IB} + [(1 - P_j)/P_j]\varepsilon_m} - \gamma^2 \right)^{-1/2}. \tag{11}$$

In the Gans estimation of LSPR peak positions, the effect of SiO_2 glass substrate must be taken into consideration. We have used the effective medium approximation of Kelly *et al.*[53] In that method, the effective dielectric constant of the medium surrounding the nanospheroids was defined as the weighted average of the dielectric constants of the substrate and of the air above the substrate, with the weight determined by the relative areas of the nanoparticle exposed to the substrate and to air.[53,54] As the dielectric constant of the SiO_2 glass substrate used in our study is 3.9, the effective dielectric constant surrounding the nanospheroids is

$$\varepsilon_m = \frac{\varepsilon_{air} + \varepsilon_{SiO_2}}{2} = 2.45, \tag{12}$$

assuming the nanostructures are half embedded in the SiO_2 substrate. Therefore, the longitudinal plasmon mode for the LSPR peak positions of $Ag_{(50\%)}$–$Au_{(50\%)}$ bimetallic nanospheroids as a function of the irradiation fluence is estimated to be shifted from 587 to 483 nm, as shown in Fig. 3(c), where the average sizes and aspect ratios obtained from SEM micrographs were used. However, the calculations overestimate the LSPR peaks for the samples with the irradiation fluences less than $7.0 \times 10^{16}\,\text{cm}^{-2}$. This is because the bimetallic nanostructures were simplified to be prolate spheroids, in which the aspect ratio is only used to characterize the shape. The shapes other than spheroid like triangle and dumbbell like nanostructures have a certain contribution to the resonance frequency, which can be verified by the large deviation of the aspect ratio obtained by lower dose irradiation ($<7.0 \times 10^{16}\,\text{cm}^{-2}$).

As mentioned previously, a shift of the LSPR peaks towards the longer wavelength (red shift) was observed when the irradiation fluence increased to $1.4 \times 10^{17}\,\text{cm}^{-2}$. This is because of the peculiar topology of the core–satellite nanostructures formed in the ion irradiated samples by producing a red shift of the LSPR absorption band.[22] As noticed in high-magnification TEM micrograph in Fig. 4(c), a halo of satellite clusters around the core nanospheroid formed in the embedded substrate. The formation of the satellite nanoclusters can be understood in terms of ballistic processes induced by the collisional cascades.[21] The Au and Ag atoms are ejected from the original alloy clusters following a ballistic process, and then diffuse into the SiO_2 matrix due to the radiation enhanced diffusion, starting the nucleation and growth where their concentration overcomes their solubility limit. Therefore, a strong coupling between the core spheroid and the satellite nanoclusters appeared, which strongly affects the local field near the core surface.[22] The GMM theory has been used to model the optical response of these strongly interacting spherical satellites with the core sphere. Mazzoldi's group has studied the optical property of such core–satellite nanostructures, in which red shifts of 20 nm and 60 nm were obtained for the Ne^+ and Kr^{++} irradiated $Ag_{0.4}Au_{0.6}$ alloyed nanoplanets in silica, respectively.[22]

Surface plasmon resonance response under different ion fluence was also tested with the 20 nm Au films on SiO_2 glass substrates. A similar tendency of surface plasmon resonance response to irradiation fluence was obtained. As the irradiation fluence increased, a shift of the LSPR peak positions toward the shorter wavelength was observed up to an irradiation fluence of $7.5 \times 10^{17}\,\text{cm}^{-2}$, and then shifted towards the longer wavelength with further irradiation (see S2 in the supplementary information[47]). Therefore, we expect that for the 100 keV Ar ion irradiation of 20 nm Ag–Au bimetallic film on SiO_2 glass substrate, the enhanced photoabsorption peak would be also shifted toward the shorter wavelength with the increase of irradiation fluence, and then shifted toward the longer wavelength with further irradiation. For the film thickness decreased to be 10 nm and the beam energy increased to be 250 keV, the ion induced blistering on the surface occurred (see S3 in the supplementary information[47]). Therefore, thicker metallic film is required to obtain similar surface plasmon resonance response under difference fluences for the higher ion beam energy.

For the $Ag_{(X\%)}$–$Au_{(100\text{-}X\%)}$ bimetallic nanospheroids with a comparable size, the peak positions for the LSPR spectra were estimated to be shifted approximately linearly from 452 to 521 nm with the increase of Au concentrations (Fig. 6(c)), which fits the tendency of the experimental data well. Also, this result is consistent with previous

works,[9,20,24,25] in which the Ag–Au alloy nanoparticles were synthesized through chemical methods. However, the calculation underestimates the shift observed in the experimental data. The most relevant factors controlling the position of the SPR absorption band are the size, shape, compositions of the nanospheroids, the dielectric constant of the matrix, and the interactions among the nanospheroids, as the extensions of the Gans theory have demonstrated. As the $Ag_{(X\%)}$–$Au_{(100-X\%)}$ bimetallic nanospheroids have a comparable size distribution and aspect ratio distribution (Fig. 6(a)), some other factors should be take into consideration. The local refractive index was increased because of the metal atoms dispersed in the dielectric matrix due to the irradiation induced forward recoiling contributes by producing a red shift of the SPR absorption band. Also, the peculiar topology of the core–satellite nanostructures formed in the ion irradiated samples has a contribution of the red shift of the SPR absorption band, as discussed previously.[22]

V. CONCLUSIONS

In this paper, Ar–ion irradiation induced surface nanostructuring of Ag–Au bimetallic films on SiO_2 substrates and their optical properties were investigated. The surface morphology was examined using a SEM equipped with an EDS, and the microstructure of the fabricated Ag–Au nanospheroids was examined using a TEM. The following conclusions were obtained:

1. As the irradiation dose increases from $4.0 \times 10^{16}\,cm^{-2}$ to $1.4 \times 10^{17}\,cm^{-2}$, the $Ag_{(50\%)}$–$Au_{(50\%)}$ bimetallic nanospheroids on the SiO_2 substrate were formed. The mean size of the nanospheroids decreases and the aspect ratio approaches unity with an increase in the irradiation fluence. This results in a shift of the LSPR peaks towards the shorter wavelength up to an irradiation fluence of $1.0 \times 10^{17}\,cm^{-2}$, which is in good agreement with the Gans calculation. The peak was then shifted towards the longer wavelength because of the strong coupling between the core spheroid and the satellite nanoclusters via ballistic processes.
2. Tuning of the LSPR frequency over a wider range has been achieved by modifying the Ag–Au molar ratios, and a remarkable LSPR peaks shifted approximately linearly towards the longer wavelength with the increase of the Au concentration has been obtained, with a tendency in good agreement with the Gans calculation. However, the calculation underestimates the shift observed in the experimental data because of the increase of the local refractive index and the peculiar topology of the core–satellite nanospheroids, both have contributions by producing a red shift of the LSPR absorption band.

In summary, ion irradiation and post-annealing can be considered as effective approaches in surface nanostructuring and, therefore, in the fabrication of photosensitive bimetallic–silica nanocomposites. Moreover, irradiation enhanced diffusion effectively burrows the nanospheroids with functionalization surfaces into the dielectric platform, and potential application use in solid-state devices is expected.

ACKNOWLEDGMENTS

This study was supported partly by the Japan Society for the Promotion of Science (JSPS) Grant-in-Aid for Scientific Research (A) #21241025. Mr. Meng thanks the Chinese Scholarship Council for stipend support to conduct this study at Hokkaido University. The authors thank Mr. K. Ohkubo, Dr. Z. Yang, Dr. Y. Yoshida, Mrs. Yamamoto, and Mr. J. Wajima for their technical assistance and helpful discussions.

[1]T. S. Ahmadi, Z. L. Wang, T. C. Green, A. Henglein, and M. A. El-Sayed, Science **272**, 1924–1925 (1996).
[2]C. J. Murphy, Science **298**, 2139 (2002).
[3]A. J. Haes, W. P. Hall, L. Chang, W. L. Klein, and R. P. Van Duyne, Nano Lett. **4**, 1029–1034 (2004).
[4]S. Lal, S. Link, and N. J. Halas, Nature Photon. **1**, 641–648 (2007).
[5]K. A. Willets and R. P. Van Duyne, Annu. Rev. Phys. Chem. **58**, 267–297 (2007).
[6]P. K. Jain, X. Huang, I. H. El-Sayed, and M. A. El-Sayed, Acc. Chem. Res. **41**, 1578–1586 (2008).
[7]J. N. Anker, W. P. Hall, O. Lyandres, N. C. Shah, J. Zhao, and R. P. Van Duyne, Nature Mater. **7**, 442–453 (2008).
[8]K. M. Mayer and J. H. Hafner, Chem. Rev. **111**, 3828–3857 (2011).
[9]M. A. Garcia, J. Phys. D: Appl. Phys. **44**, 283001 (2011).
[10]P. Zijlstra, P. M. R. Paulo, and M. Orrit, Nat. Nanotechnol. **7**, 379–382 (2012).
[11]A. G. Brolo, "Plasmonics for future biosensors," Nature Photon. **6**, 709–713 (2012).
[12]V. G. Kravets, F. Schedin, R. Jalil, L. Britnell, R. V. Gorbachev, D. Ansell, B. Thackray, K. S. Novoselov, A. K. Geim, A. V. Kabashin, and A. N. Grigorenko, Nature Mater. **12**, 304–309 (2013).
[13]C. Bohren and D. Huffman, *Absorption and Scattering of Light by Small Particles* (Wiley, New York, 1998).
[14]B. T. Draine and P. J. Flatau, J. Opt. Soc. Am. A **11**, 1491–1499 (1994).
[15]P. K. Jain, K. S. Lee, I. H. El-Sayed, and M. A. El-Sayed, J. Phys. Chem. B **110**, 7238–7248 (2006).
[16]W. Y. Ma, H. Yang, J. P. Hilton, Q. Lin, J. Y. Liu, L. X. Huang, and J. Yao, Opt. Express **18**, 843–853 (2010).
[17]S.-J. Chen, F. C. Chien, G. Y. Lin, and K. C. Lee, Opt. Lett. **29**, 1390–1392 (2004).
[18]K.-S. Lee and M. A. El-Sayed, J. Phys. Chem. B **109**, 20331–20338 (2005).
[19]K.-S. Lee and M. A. El-Sayed, J. Phys. Chem. B **110**, 19220–19225 (2006).
[20]L. M. Liz-Marzan, Langmuir **22**, 32–41 (2006).
[21]G. Mattei, V. Bello, P. Mazzoldi, G. Pellegrini, C. Sada, C. Maurizio, and G. Battaglin, Nucl. Instrum. Methods Phys. Res. B **240**, 128–132 (2005).
[22]G. Pellegrini, V. Bello, G. Mattei, and P. Mazzoldi, Opt. Express **15**, 10097–10102 (2007).
[23]H. Sun, M. Yu, G. Wang, X. Sun, and J. Lian, J. Phys. Chem. C **116**, 9000–9008 (2012).
[24]S. Link, Z. L. Wang, and M. A. El-Sayed, J. Phys. Chem. B **103**, 3529–3533 (1999).
[25]D. Barreca, A. Gasparotto, C. Maragno, E. Tondello, and S. Gialanella, J. Nanosci. Nanotechnol. **7**, 2480–2486 (2007).
[26]R. Kuladeep, L. Jyothi, K. Shadak Alee, K. L. N. Deepak, and D. Narayana Rao, Opt. Mater. Express **2**, 161–172 (2012).
[27]S. Kruss, V. Srot, P. A. Van Aken, and J. P. Spatz, Langmuir **28**, 1562–1568 (2012).
[28]Y. Kojima and T. Kato, Nanotechnology **19**, 255605 (2008).
[29]C. M. Müller, F. C. F. Mornaghini, and R. Spolenak, Nanotechnology **19**, 485306 (2008).
[30]Y. Yoshida, S. Watanabe, Y. Nishijima, K. Ueno, H. Misawa, and T. Kato, Nanotechnology **22**, 375607 (2011).
[31]S. Budak, S. Guner, R. Amaral Micanisawa, C. Muntele, and D. Ila, Nucl. Instrum. Methods Phys. Res. B **266**, 1574–1577 (2008).
[32]O. Peña, U. Pal, L. Rodríguez-Fernández, H. G. Silva-Pereyra, V. Rodríguez-Iglesias, J. C. Cheang-Wong, J. Arenas-Alatorre, and A. Oliver, J. Phys. Chem. C **113**, 2296–2300 (2009).
[33]J. Prakash, A. Tripathi, V. Rigato, J. C. Pivin, J. Tripathi, K. H. Chae, S. Gautam, P. Kumar, K. Asokan, and D. K. Avasthi, J. Phys. D: Appl. Phys. **44**, 125302 (2011).

[34]L. Repetto, B. Š. Batič, G. Firpo, E. Piano, and U. Valbusa, Appl. Phys. Lett. **100**, 223113 (2012).
[35]X. Meng, T. Shibayama, R. Yu, S. Takayanagi, and S. Watanabe, J. Mater. Sci. **48**, 920–928 (2013).
[36]K. Neubeck, C.-E. Lefaucheur, H. Hahn, A. G. Balogh, H. Baumann, K. Bethge, and D. M. Rück, Nucl. Instrum. Methods Phys. Res. B **106**, 589–596 (1995).
[37]X. Hu, D. G. Cahill, and R. S. Averback, J. Appl. Phys. **92**, 3995–4000 (2002).
[38]A. Klimmer, P. Ziemann, J. Biskupek, U. Kaiser, and M. Flesch, Phys. Rev. B **79**, 155427 (2009).
[39]M. Hillenkamp, G. D. Domenicantonio, O. Eugster, and C. Félix, Nanotechnology **18**, 015702 (2007).
[40]G. Valverde-Aguilar, J. A. García-Macedo, V. M. Rentería-Tapia, R. W. Gómez, and M. Quintana-García, J. Nanopart. Res. **13**, 4613–4622 (2011).
[41]N. Alissawi, V. Zaporojtchenko, T. Strunskus, I. Kocabas, V. S. K. Chakravadhanula, L. Kienle, D. Garbe-Schönberg, and F. Faupel, Gold Bull. **46**, 3–11 (2013).
[42]S. Besner and M. Meunier, J. Phys. Chem. C **114**, 10403–10409 (2010).
[43]J. F. Ziegler, J. P. Biersack, and U. Littmark, *SRIM—The Stopping and Range of Ions in Solids* (Pergamon Press, New York, 1985 (new edition in 2009)).
[44]N. Sakaguchi, H. Kinoshita, S. Watanabe, Y. Sueishi, N. Akasaka, and H. Takahashi, J. Nucl. Mater. **382**, 197–202 (2008).
[45]C. D. Marshall, J. A. Speth, and S. A. Payne, J. Non-Cryst. Solids **212**, 59–73 (1997).
[46]C. V. Thompson, Annu. Rev. Mater. Res. **42**, 399–434 (2012).
[47]See supplementary material at http://dx.doi.org/10.1063/1.4817725 for Ag nanospheroids oxidation (S1), surface plasmon response of 20 nm Au film on SiO_2 substrate under Ar ion irradiation (S2), and surface plasmon response of 10 nm Au film on SiO_2 substrate under Ar ion irradiation (S3).
[48]M. Futamata, Y. Maruyama, and M. Ishikawa, J. Phys. Chem. B **107**, 7607–7617 (2003).
[49]V. I. Belotelov, G. Carotenuto, L. Nicolais, A. Longo, G. P. Pepe, P. Perlo, and A. K. Zvezdin, J. Appl. Phys. **99**, 044304 (2006).
[50]M. Quinten, Z. Phys. B **101**, 211–217 (1996).
[51]S. Berciaud, L. Cognet, P. Tamarat, and B. Lounis, Nano Lett. **5**, 515–518 (2005).
[52]W. Chen, K. P. Chen, M. D. Thoreson, A. V. Kildishev, and V. M. Shalaev, Appl. Phys. Lett. **97**, 211107 (2010).
[53]K. L. Kelly, E. Coronado, L. L. Zhao, and G. C. Schatz, J. Phys. Chem. B **107**, 668–677 (2003).
[54]G. H. Chan, J. Zhao, G. C. Schatz, and R. P. Van Duyne, J. Phys. Chem. C **112**, 13958–13963 (2008).